Atmos. Chem. Phys. Discuss., 14, 12377–12408, 2014
www.atmos-chem-phys-discuss.net/14/12377/2014/
doi:10.5194/acpd-14-12377-2014

Atmospheric Chemistry and Physics Discussions
Open Access

Summertime tropospheric ozone assessment over the Mediterranean region using the thermal infrared IASI/MetOp sounder and the WRF-Chem model

S. Safieddine[1], A. Boynard[1], P.-F. Coheur[2], D. Hurtmans[2], G. Pfister[3], B. Quennehen[1], J. L. Thomas[1], J.-C. Raut[1], K. S. Law[1], Z. Klimont[4], J. Hadji-Lazaro[1], M. George[1], and C. Clerbaux[1,2]

[1]Sorbonne Universités, UPMC Univ. Paris 06, Université Versailles St-Quentin; CNRS/INSU, LATMOS-IPSL, Paris, France
[2]Spectroscopie de l'Atmosphère, Chimie Quantique et Photophysique, Université Libre de Bruxelles (U.L.B.), Brussels, Belgium
[3]Atmospheric Chemistry Division, National Center for Atmospheric Research, Boulder, Colorado, USA
[4]International Institute for Applied Systems Analysis, Laxenburg 2361, Austria

Received: 7 March 2014 – Accepted: 1 May 2014 – Published: 14 May 2014

Correspondence to: S. Safieddine (sarah.safieddine@latmos.ipsl.fr)

Published by Copernicus Publications on behalf of the European Geosciences Union.

Abstract

Over the Mediterranean region, elevated tropospheric ozone (O_3) values are recorded, especially in summer. We use the Infrared Atmospheric Sounding Interferometer (IASI) and the Weather Research and Forecasting Model with Chemistry (WRF-Chem) to understand and interpret the factors and emission sources responsible for the high O_3 concentrations observed in the Mediterranean troposphere. Six years of IASI data have been analyzed and show consistent maxima during summer, with an increase of up to 22 % in the [0–8] km O_3 column in the eastern part of the basin compared to the middle of the basin. We analyze 2010 as an example year to investigate the processes that contribute to these summer maxima. Using two modeled O_3 tracers (inflow to the model domain and local anthropogenic emissions), we show that between the surface and 2 km, O_3 is mostly formed from anthropogenic emissions and above 4 km, is mostly transported from outside the domain. Evidence of stratosphere to troposphere exchanges (STE) in the eastern part of the basin is shown, and corresponds with low relative humidity and high potential vorticity.

1 Introduction

Tropospheric ozone (O_3) is a greenhouse gas, air pollutant, and a primary source of the hydroxyl radical OH, the most important oxidant in the atmosphere (Chameides and Walker, 1973; Crutzen, 1973). Previous observations and studies have shown that tropospheric O_3 over the Mediterranean exhibits a significant increase during summer time, especially in the east of the basin (Kouvarakis et al., 2000; Im et al., 2011; Gerasopoulos et al., 2005, 2006; Richards et al., 2013; Zanis et al., 2014). Meteorological conditions such as frequent clear sky conditions (Fig. 1a) and high exposure to solar radiation (Fig. 1b) in summer enhance the formation of photochemical O_3 due to the availability of its precursors. These precursors include carbon monoxide (CO), peroxyl radicals generated by the photochemical oxidation of volatile organic compounds

ACPD
14, 12377–12408, 2014

(VOCs) and nitrogen oxides ($NO_x = NO + NO_2$). Locally, the basin is surrounded with megacities such as Cairo, Istanbul, and Athens that are large sources of local anthropogenic emissions. The geographic location of the basin makes it a receptor for anthropogenic pollution from Europe both in the boundary layer (Fig. 1c) and the mid-troposphere (Fig. 1d) as the region is located under the effect of westerlies in winter and the descending branch of the Hadley circulation in summer (Bolle, 2002). Moreover, the Asian monsoon region can induce a Rossby-wave pattern to the west, causing mid-latitude warm air to descend adiabatically in particular over the Mediterranean (Rodwell and Hoskins, 1996). This can be major contributor to climate extreme events, such as the 2010 Russian heat wave (Schubert et al., 2011) that caused severe fires with high O_3 precursors emissions (R'Honi et al., 2013). The threshold O_3 value for air quality standards in Europe (of daily maximum of running 8 h mean values of 60 ppbv) is exceeded on more than 25 days per year at a large number of stations across Europe, many of which are located to the south of Europe in the Mediterranean Basin (EEA, 2012). Different explanation about the source of the O_3 maxima are found in the literature: for example, Lelieveld et al. (2002) showed that in the upper troposphere, Asian pollution is transported from the east by the monsoon across the Mediterranean tropopause into the lower stratosphere. Gerasopoulos et al. (2005) have shown that the mechanism that controls surface O_3 seasonal variability in the eastern basin during summer is mainly the transport from Europe. Galani et al. (2003) detected with lidar measurements an increase of 10 % of tropospheric O_3 between 4.5 and 6.5 km due to stratosphere to troposphere exchange events (STE). Zbinden et al. (2013) using aircraft data from MOZAIC (Measurements of OZone and water vapour by in-service AIrbus airCraft programme) over 15 years (1994–2009), showed that the tropospheric O_3 columns in the east of the Mediterranean, reached a maximum reaching 43.2 DU during June-July. This recorded maximum exceeds the maximum recorded for Beijing for the same period, for example. Model calculation using WRF-Chem (Weather Research and Forecasting model coupled with Chemistry) and EMEP (European Monitoring and Evaluation Programme) MSC-W (Meteorological Synthesizing Centre-West)

ACPD
14, 12377–12408, 2014

models of the Eastern Mediterranean during heat waves in 2007 showed that the daily maximum near surface O_3 is mostly sensitive to anthropogenic emissions of O_3 precursors (Hodnebrog et al., 2012). Im et al. (2011) found that the near surface ozone mixing ratios increases almost linearly with temperature by 1.0 ± 0.1 ppb O_3 per Kelvin. STE processes can affect the tropospheric O_3 budget and impact air quality if transported to the boundary layer (Fiore et al., 2002). Stratospheric intrusions have been detected in the Mediterranean region, especially to the east side (Galani et al., 2003; Zanis et al., 2014), because it lies to the south of the North Hemisphere polar jet flowing over mid-latitudes (Stohl et al., 2000; Gerasopoulos et al., 2001). Understanding the factors that contribute to the O_3 maxima is important for developing control measures and prevents pollution build up. In this study we analyze O_3 and its sources at different altitudes in the Mediterranean atmosphere. Section 2 introduces the model and observations data sets used in this study. In Sect. 3, we analyze six years of IASI tropospheric O_3 seasonal variation above the Mediterranean. In Sect. 4 we focus on summer 2010, as an example year, and validate the WRF-Chem model simulation with surface O_3 and IASI data, and then use the WRF-Chem model to assess the sources of O_3 in the troposphere. In Sect. 5, we use IASI and WRF-Chem free tropospheric O_3 data to investigate potential stratosphere to troposphere exchange events. Conclusions are given in Sect. 6.

2 Model and observational data

2.1 WRF-Chem model

In this study, we use the regional chemistry transport model WRF-Chem, Version 3.2 (Grell et al., 2005) to assess the O_3 budget and spatio-temporal variability of O_3 over the Mediterranean during summer 2010. The model domain is centered over the Mediterranean Basin covering most of Europe at 50 km × 50 km horizontal resolution with 28 vertical levels between the surface and 10 hPa. The meteorological initial and

ACPD
14, 12377–12408, 2014

boundary conditions are based on the National Centers for Environmental Prediction (NCEP) Final (FNL) analyses with analysis nudging for wind, temperature, and humidity applied. Fields are provided every 6 h with 1° horizontal resolution and 27 vertical levels from the surface up to 10 hPa. The chemical initial and boundary conditions, spatially and temporally varying (6 h), are constrained by global chemical transport simulations from MOZART-4/GEOS-5 with 1.9° × 2.5° horizontal resolution (Emmons et al., 2010a). The WRF-Chem gas-phase chemical mechanism is that from Model for Ozone and Related Chemical Tracers, version 4 (MOZART-4) (Emmons et al., 2010a), which is coupled to the aerosol scheme Goddard Chemistry Aerosol Radiation and Transport (GOCART) model (Chin et al., 2002). The model also includes anthropogenic and fire emissions that are calculated off-line. The anthropogenic emissions used within the WRF-Chem model were developed in the frame of the ECLIPSE European project using the Greenhouse gas and Air pollution Interactions and Synergies (GAINS) model. In addition to the ECLIPSE V4.0 anthropogenic emissions, ship emissions from the RCP 6.0 scenario (Fujino et al., 2006; Hijioka et al., 2008) were used. Biomass burning emissions are obtained from the Fire Inventory from NCAR (FINN V1) (Wiedinmyer et al., 2011). Biogenic emissions are calculated online from the Model of Emissions of Gases and Aerosols from Nature (MEGAN) (Guenther et al., 2006). The WRF-Chem simulation outputs are saved every 2 h from 1 June 2010 until 31 August 2010.

In this study, we use a tagging method for O_3 (Emmons et al., 2012), which has been applied in global models for diagnosing contributions for individual sources to O_3 (e.g. Lamarque et al., 2005; Pfister et al., 2006, 2008; Emmons et al., 2010b; Wespes et al., 2012), and in a regional chemical transport model (although not in WRF-Chem) over China (Ma et al., 2002). Recently, this scheme was used for the first time in the WRF-Chem model to quantify the contribution of inflow on surface O_3 over California (Pfister et al., 2013). Here, we apply this scheme to keep track of the contribution of O_3 within the WRF-Chem domain. To determine O_3 sources, tagged NO_x is traced through the odd nitrogen species (e.g. PAN, HNO_3, organic nitrates) to account for NO_x recycling (Emmons et al., 2012). Two separate tracer runs were conducted with the same emis-

ACPD
14, 12377–12408, 2014

sions, initial, and boundary conditions. In the first one, $O_{3_{anthro}}$ tracer accounts for the anthropogenic regional tagged NO_x, while the second one $O_{3_{inflow}}$ tracer accounts for tagged O_3 as well as all nitrogen species at the lateral boundaries of the regional model domain. $O_{3_{inflow}}$ tracer includes O_3 and O_3 precursors from all natural (including lightning and stratospheric O_3) and anthropogenic sources outside the regional modeling domain. Within the regional modeling domain, $O_{3_{inflow}}$ undergoes transport and chemical processes, but is not produced from sources other than from reactions including the tagged species. Since in this version of WRF-Chem the stratospheric O_3 is controlled by the lateral boundaries, O_3 from stratospheric intrusions within the regional domain would be labeled as $O_{3_{inflow}}$ as well. More details about the tagging scheme are provided in Emmons et al. (2012). Two more tracers are available to complete the O_3 budget: O_3 from biogenic sources and O_3 from fires. Given that their contribution to the total budget in comparison with INFLOW and ANTHRO tracers is very small, they are not analyzed in this study.

2.2 EMEP data

The EMEP (European Monitoring and Evaluation Programme) O_3 hourly data (http://ebas.nilu.no/) are used to validate the WRF-Chem model at the surface. In this study, measurements at 8 rural background sites during the summer of 2010 are used. Details on the EMEP observation system can be found in Hjellbrekke et al. (2012). The geographic location of the 8 stations used for validation is plotted in Fig. 2 and the corresponding details are listed in Table 1. Two more station data were available, GR01-Aliartos (38.37° N, 23.11° E) and IT01-Montelibretti (42.1° N, 12.63° E). We disregarded the data from these stations because they show strong diurnal variation of 80–90 ppbv amplitude, and recurrent near zero O_3 concentrations throughout the period of the study, and were thus considered unreliable.

ACPD
14, 12377–12408, 2014

2.3 IASI satellite measurements

On board of the MetOp platforms, IASI was launched in October 2006 (IASI-1) and September 2012 (IASI-2). It has been sounding operationally the atmosphere since June 2007 (IASI-1) and January 2013 (IASI-2). IASI is a nadir looking Fourier transform spectrometer that probes the Earth's atmosphere in the thermal infrared spectral range between 645 and 2760 cm^{-1}, with a spectral resolution of 0.5 cm^{-1} (apodized) and 0.25 cm^{-1} spectral sampling. Global distributions of O_3 vertical profiles are retrieved in near real time using a dedicated radiative transfer and retrieval software for the IASI O_3 product, the Fast Optimal Retrievals on Layers for IASI (FORLI-O_3) (Hurtmans et al., 2012). The IASI FORLI-O_3 observations are selected for scenes with cloud coverage below 13 %, and with RMS of the spectral fit residual lower than 3.5×10^{-8} $W\,cm^2\,sr\,cm^{-1}$. Details about the chemical components that can be measured by IASI can be found in Clerbaux et al. (2009), Coheur et al. (2009), Turquety et al. (2009), and Clarisse et al. (2011). IASI has the highest O_3 sensitivity in the mid to upper troposphere (Safieddine et al., 2013). Figure 3 shows the partial column averaging kernel function for two specific observations above land and sea during June 2010. It can be seen that the sensitivity to the O_3 profile is maximal around 4–10 km for both observations. IASI sensitivity near the surface is usually limited above the sea, as seen on the right panel of Fig. 3, and better over land as seen in the left panel, and with corresponding better thermal contrast (7.8° above land, and 1.2° above sea). In fact, IASI is able to detect several pollutants especially when large thermal contrast is combined with stable meteorological conditions leading to the accumulation of pollutants near the surface (Boynard et al., 2014).

3 Tropospheric O_3 seasonal variation as seen by IASI

To investigate the seasonal behavior of tropospheric O_3 above the Mediterranean, we plot in Fig. 4 the [0–8] km tropospheric O_3 column as seen by IASI, during the 6 years of

ACPD
14, 12377–12408, 2014

IASI observations available. The data were averaged over 3 months to better represent the different seasons. We use daytime observations only since the information content of IASI-O_3 data is shown to be higher during the day (Clerbaux et al., 2009). We observe a similar tropospheric O_3 seasonal behavior each year. The weakest values are observed in winter (DJF) and autumn (SON), when solar activity is minimal. Increasing values in spring (MAM) is due to the increase of O_3 production from photochemistry, buildup of winter O_3 and its precursors, transport, and/or from O_3 of stratospheric origin integrating into the troposphere, as spring is the season known for stratosphere to troposphere exchange events (Levy et al., 1985; Logan, 1985; Holton et al., 1995). The [0–8] km column reaches a maximum in summer (JJA) due to high photochemical O_3 production, horizontal transport into the region, or stratosphere to troposphere exchange, all of which will be investigated in detail in the following sections. Richards et al. (2013) detected a similar spatial distribution with the Global Ozone Monitoring Experiment-2 (GOME-2) during summers of 2007 and 2008, with values exceeding 32 DU at the east of the basin for the [0–6] km O_3 column. To investigate further the higher values detected to the east of the basin, we analyze longitudinal strips of 1° width along 15° E and 30° E, marked in grey in the last panel of Fig. 4.

Figure 5 shows that during the period of 2008 to 2013, the summers in the east of the basin, notably at 30° E (plotted in red) are marked by elevated tropospheric O_3 values, up to 30 Dobson units (DU) in July 2010 and exceeding those at 15° E (plotted in black). The difference between the two O_3 columns at the 2 different longitudes was highest (4.7 DU-22 %) during June 2012.

4 O_3 budget from the WRF-Chem model during summer 2010

From this section onwards, we focus our analysis on summer 2010, which is a typical summer in the 2008–2013 period as seen in Figs. 4 and 5, and corresponds to the year for which we have used the anthropogenic emission inventory in the model.

ACPD
14, 12377–12408, 2014

4.1 Model evaluation: comparison to EMEP and IASI

In order to validate and evaluate the model, we use the surface O_3 data from the EMEP stations (Sect. 2.2), then free tropospheric O_3 data from IASI (Sect. 2.3).

4.1.1 Comparison to EMEP surface monitoring stations

Linear spatial interpolation was applied to WRF-Chem data in order to correlate the model outputs and the EMEP data that were averaged every 2 h to coincide with the model run output data.

Figure 6a shows the individual time series of the data of the 8 stations used for the validation. Figure 6b shows the correlation between EMEP data and the WRF-Chem simulations for the period JJA 2010. The model reproduces reasonably well the average amplitude of the daily cycle seen in the observation. The model underestimates, however, the surface observation during all the summer period with a mean bias of 4.13 ppbv (6 %) as seen in panel (b). This underestimation may be due to the resolution of the model which is around $0.5^\circ \times 0.5^\circ$ resulting in a grid that is larger than the EMEP rural sites and includes other surface O_3 contributions. Other possible reasons include difficulties in simulating local flow patterns due to topography and land–sea circulation, uncertainties in emissions and NO_x concentrations (Pfister et al., 2013). The model simulates the bi-hourly surface O_3 with a correlation ranging from 0.41 to 0.79 and a mean value of 0.52. Our results compare well with the study by Tuccella et al. (2012) that compared WRF-Chem to 75 EMEP stations over Europe during 2007, and found that hourly O_3 exhibit a correlation with observations ranging from 0.38 to 0.83. The largest discrepancy observed, with modeled O_3 values larger than 80 ppbv, is for the station ES06-Mahon (39.87° N, 4.32° E), which might be due a particular uncertainty in the model emissions or dry deposition over this area.

ACPD
14, 12377–12408, 2014

4.1.2 Comparison to IASI observations

Averaged data for summer 2010 are used for the comparison of WRF-Chem and IASI O_3 free tropospheric column. The modeled profile is first linearly interpolated to the time and location of the retrieval. Then, the averaging kernels associated with each IASI measurement and its apriori profile are applied to the interpolated modeled profile. Figure 7 shows the spatial distribution of the [4–10] km integrated IASI and WRF-Chem model O_3 column along with the relative differences. We chose to analyze this part of the atmosphere in particular because IASI has a better sensitivity between 4 and 10 km over both land and water as shown in Fig. 3. The model reproduces well the spatial patterns seen by IASI during summer (JJA) 2010, with a correlation coefficient of about 0.93 and a summertime mean bias of 6.1 ppbv (25 %) (not shown). The model underestimation of the [4–10] km O_3 column might due to the difficulties in resolving the high O_3 concentrations observed in transported plumes over large distances (Pfister et al., 2013). On the other hand, the high discrepancies seen over northern Africa, might be due to IASI poor spectral fits above surfaces with sharp emissivity variations particularly above the desert (Hurtmans et al., 2012), leading to a possible overestimation of the real profile. We analyzed the IASI columnar total error relative to measurement for the [4–10] km integrated partial column and we found that it is on average around 7 % in the model domain, and between 7 and 12 % where the discrepancies between the model and IASI are the highest.

4.2 Origins of boundary layer O_3 over the Mediterranean

Modeled O_3 concentrations are illustrated in Fig. 8a–c at the surface, 1 and 2 km during JJA 2010. At the surface, modeled O_3 exhibits the highest values downwind the European continent.

At 1 and 2 km the whole eastern part of the basin is characterized by high O_3 mixing ratios. In order to investigate possible sources of high O_3, we run the model with 2 different tracers of pollution: $O_{3_{anthro}}$ and $O_{3_{inflow}}$ as described in Sect. 2.1. $O_{3_{anthro}}$ (Fig. 8d–

ACPD
14, 12377–12408, 2014

f) assesses the possible anthropogenic contribution of O_3 at different altitudes, while $O_{3_{inflow}}$ (Fig. 8g–i), provides an estimate of transport of O_3 from outside the study region (the entire model study domain from surface to 10 hPa) including the stratosphere. The residual plots calculated as $100\,\% - (O_{3_{anthro}}\,\% + O_{3_{inflow}}\,\%)$ and plotted in panels (j–l) show that these two tracers contribution provide most of the O_3 budget over the model domain, at the different altitudes of Figs. 8 and 9. The surface shows a high contribution for the anthropogenic emission tracer ($O_{3_{anthro}} > 85\,\%$), with almost zero contribution of the inflow tracer. This shows the importance of local emissions to the O_3 surface concentration. At 1 km, the highest contribution is also for the anthropogenic tracer (up to 75–80 %), whereas the result is mixed at 2 km between the 2 tracers (around 50–60 % for $O_{3_{anthro}}$ and 40–50 % for $O_{3_{inflow}}$), suggesting that up to 50 % of the O_3 available at 2 km is being transported. The rest of the O_3 plotted in the residual plots (panels j–l) and decreasing with altitude is suggested to be from fire sources, as the extended domain used in the study includes the Russian fires of summer 2010. Moreover, the residual could also come, to a lesser extent, from biogenic sources especially over land.

4.3 Origins of free tropospheric O_3 over the Mediterranean

O_3 concentrations at 4, 6 and 8 km in Fig. 9a–c show that the eastern part of the basin is subject to much higher O_3 values, reaching up to 100 ppbv between 6 and 8 km (see further discussion in Sect. 5). The anthropogenic contribution decreases with altitude, whereas the O_3 inflow contribution increases. The northeastern corner of the modeled domain in panels (d–f) show anthropogenic contribution between 20 and 40 %. This might be due to important vertical transport and mixing in the free troposphere. Panels (g–i) show that 70 to 100 % of the available O_3 between 4 and 8 km does not come from local sources. The high values are likely due to long-range transport of pollution from outside the study region or transport of air masses from the stratosphere that we will discuss in the following section. The low values recorded in the residual plots in panels

ACPD
14, 12377–12408, 2014

(j–l) show that the O_3 budget in the free troposphere over this region is controlled almost exclusively by local anthropogenic sources and transport.

5 WRF-Chem and IASI detection of stratosphere–troposphere exchange events

Figures 4, 5 and 9a–c showed that the eastern part of the Mediterranean Basin in summer is subject to high O_3 mixing ratios at 4, 6 and 8 km. In order to further investigate the sources and processes responsible for these enhancements, modeled and observed IASI O_3 vertical profiles in the troposphere were examined, during summer 2010, to try to detect possible stratosphere to troposphere exchange (STE) events.

Figure 10 shows the tropospheric O_3 vertical distributions along 15° E (mid-Mediterranean) and 30° E (eastern Mediterranean) for IASI (panels a and b) and WRF-Chem, smoothed with the IASI averaging kernels (panels c and d) for JJA 2010. Between 4 and 8 km, panels (b) and (d) show higher values of O_3 in the eastern part of the basin (30° E) with concentrations ranging between 50 and 100 ppbv for IASI and 40 to 100 ppbv for WRF-Chem (WRF-Chem underestimates IASI as shown in Fig. 7).

To identify the cause of the high free tropospheric O_3 values, we plot in Fig. 11 the potential vorticity (PV) and relative humidity (RH) between 350 and 250 hPa from the WRF-Chem model. PV and RH measurements can be used as markers of transport from the upper troposphere-lower stratosphere (UTLS) to the troposphere: elevated O_3 and PV, and low RH values, would indicate that high free troposphere values are due to downward transport from the UTLS (Holton et al., 1995). Figure 11 shows that the highest PV values (0.8 to 1.4 pvu) (potential vorticity unit, 1 pvu = $10^{-6}\,m^2\,K^{-1}\,kg^{-1}\,s^{-1}$), and the lowest RH values (5–15 %) are recorded to the east of the basin, while lower PV values are recorded in the mid and to the west of the basin (0.6–0.9), with higher RH values (20–60 %). The high PV/low RH values to the east are in accordance with Figs. 9 and 10, strongly suggesting that this part of the basin is subject to transport from the UTLS into the free troposphere. In fact, at 30° E and around 37–39° N (panels b and d of Fig. 10) both IASI and the model observe a stratospheric intrusion. It corresponds

ACPD
14, 12377–12408, 2014

to PV > 1.2 pvu and RH < 20 %. In a recent study, Zanis et al. (2014) using 12 year climatology (1998–2009) of the ERA-interim reanalysis, also detected frequent events of STE with PV ranging between 0.4 and 1.4 pvu between 750 and 250 hPa during July and August to the east of the basin, in accordance with our results for summer 2010.

6 Conclusions

Six years of tropospheric O_3 observations provided by the IASI mission above the Mediterranean are shown. Tropospheric O_3 shows a consistent seasonal behavior over the period 2008–2013 with pronounced maxima in summer. Since IASI has a lower sensitivity in the lower troposphere and above the sea, anthropogenic emission contribution to the boundary layer O_3 is not well captured by the instrument. However, IASI is able to detect in the free to upper troposphere, where its sensitivity is the highest, high tropospheric O_3 values to the east of the basin during the 6 years. Focusing on summer 2010, we use IASI and WRF-Chem model together to interpret these maxima. Our results show that the summer O_3 maxima over the region, especially in the eastern part of the basin are due to 3 main factors. (1) High local anthropogenic emissions that are responsible to 80–100 % of O_3 in the boundary layer (surface–2 km), as demonstrated by the anthropogenic O_3 tracer of the WRF-Chem model; (2) important vertical and horizontal transport of O_3 in the free troposphere as seen by the pollution inflow tracer of the WRF-Chem model responsible of 70–100 % of O_3 at 4, 6 and 8 km; and (3) evidence of stratosphere to troposphere exchange events, particularly in the eastern part of the basin as seen by the model as well as the IASI instrument and confirmed by high potential vorticity and low humidity.

This study shows the ability of infrared instruments, such as IASI, to detect seasonal variations of tropospheric O_3 as well as STEs. It also shows that in order to understand the possible sources of the tropospheric O_3 maxima seen in the Mediterranean region in summer, it is important to quantify and analyze O_3 separately at different altitudes in the atmosphere. Furthermore, it shows that the use of model O_3 tracers is valuable

ACPD
14, 12377–12408, 2014

for identifying different O_3 sources and the factors driving O_3 variations at the scale of interest for air quality applications.

Acknowledgements. IASI is a joint mission of EUMETSAT and the Centre National d'Etudes Spatiales (CNES, France). The IASI L1 data are distributed in near real time by EUMETSAT through the EumetCast system distribution. The authors acknowledge the French Ether atmospheric database (www.pole-ether.fr) for providing the IASI L1C data and L2 temperature data. This work was undertaken under the auspices of the O3M-SAF project of the EUMETSAT. The French scientists are grateful to CNES and Centre National de la Recherche Scientifique (CNRS) for financial support. The research in Belgium is funded by the Belgian State Federal Office for Scientific, Technical and Cultural Affairs and the European Space Agency (ESA Prodex arrangement). P. F. Coheur is Senior Research Associate with F.R.S-FNRS. Support is also acknowledged from the EU FP7 ECLIPSE (Evaluating the Climate and Air Quality Impacts of Short-Lived Pollutants) project (no. 282688).

References

Bolle, H.-J. (Ed.): Mediterranean Climate: Variability and Trends, Springer-Verlag, Berlin, 2002.

Boynard, A., Clerbaux, C., Clarisse, L., Safieddine, S., Pommier, M., Van Damme, M., Bauduin, S., Oudot, C., Hadji-Lazaro, J., Hurtmans, D., and Coheur, P.-F.: First simultaneous space measurements of atmospheric pollutants in the boundary layer from IASI: a case study in the North China Plain, Geophys. Res. Lett., 41, 645–651, doi:10.1002/2013GL058333, 2014.

Chameides, W. and Walker, J. C. G.: A photochemical theory of tropospheric ozone, J. Geophys. Res., 78, 8751–8760, 1973.

Chin, M., Ginoux, P., Kinne, S., Torres, O., Holben, B. N., Duncan, B. N., Martin, R. V., Logan, J. A., Higurashi, A., and Nakajima, T.: Tropospheric aerosol optical thickness from the GOCART model and comparisons with satellite and Sun photometer measurements, J. Atmos. Sci., 59, 461–483, 2002.

Clarisse, L., R'Honi, Y., Coheur, P.-F., Hurtmans, D., and Clerbaux, C.: Thermal infrared nadir observations of 24 atmospheric gases, Geophys. Res. Lett., 38, L10802, doi:10.1029/2011GL047271, 2011.

Clerbaux, C., Boynard, A., Clarisse, L., George, M., Hadji-Lazaro, J., Herbin, H., Hurtmans, D., Pommier, M., Razavi, A., Turquety, S., Wespes, C., and Coheur, P.-F.: Monitoring of atmospheric composition using the thermal infrared IASI/MetOp sounder, Atmos. Chem. Phys., 9, 6041–6054, doi:10.5194/acp-9-6041-2009, 2009.

Coheur, P.-F., Clarisse, L., Turquety, S., Hurtmans, D., and Clerbaux, C.: IASI measurements of reactive trace species in biomass burning plumes, Atmos. Chem. Phys., 9, 5655–5667, doi:10.5194/acp-9-5655-2009, 2009.

Crutzen, P. J.: A discussion of the chemistry of some minor constituents in the stratosphere and troposphere, Pure Appl. Geophys., 106–108, 1385, 1973.

EEA: Air Quality in Europe – 2012 Report, European Environment Agency, ISBN 978-92-9213-328-3, Luxembourg, Office for Official Publications of the European Union, doi:10.2800/55823, 2012.

Emmons, L. K., Walters, S., Hess, P. G., Lamarque, J.-F., Pfister, G. G., Fillmore, D., Granier, C., Guenther, A., Kinnison, D., Laepple, T., Orlando, J., Tie, X., Tyndall, G., Wiedinmyer, C., Baughcum, S. L., and Kloster, S.: Description and evaluation of the Model for Ozone and Related chemical Tracers, version 4 (MOZART-4), Geosci. Model Dev., 3, 43–67, doi:10.5194/gmd-3-43-2010, 2010a.

Emmons, L. K., Apel, E. C., Lamarque, J.-F., Hess, P. G., Avery, M., Blake, D., Brune, W., Campos, T., Crawford, J., DeCarlo, P. F., Hall, S., Heikes, B., Holloway, J., Jimenez, J. L., Knapp, D. J., Kok, G., Mena-Carrasco, M., Olson, J., O'Sullivan, D., Sachse, G., Walega, J., Weibring, P., Weinheimer, A., and Wiedinmyer, C.: Impact of Mexico City emissions on regional air quality from MOZART-4 simulations, Atmos. Chem. Phys., 10, 6195–6212, doi:10.5194/acp-10-6195-2010, 2010b.

Emmons, L. K., Hess, P. G., Lamarque, J.-F., and Pfister, G. G.: Tagged ozone mechanism for MOZART-4, CAM-chem and other chemical transport models, Geosci. Model Dev., 5, 1531–1542, doi:10.5194/gmd-5-1531-2012, 2012.

Fiore, A. M., Jacob, D. J., Bey, I., Yantosca, R. M., Field, B. D., Fusco, A. C., and Wilkinson, J. G.: Background ozone over the United States in summer: origin, trend, and contribution to pollution episodes, J. Geophys. Res., 107, 4275, doi:10.1029/2001JD000982, 2002.

Fujino, J., Nair, R., Kainuma, M., Masui, T., and Matsuoka, Y.: Multi-gas mitigation analysis on stabilization scenarios using AIM global model, multigas mitigation and climate policy, Energ. J., 27, 343–353, 2006.

ACPD
14, 12377–12408, 2014

Galani, E., Balis, D., Zanis, P., Zerefos, C., Papayannis, A., Wernli, H., and Gerasopoulos, E.: Observations of stratosphere–troposphere transport events over the eastern Mediterranean using a ground-based lidar system, J. Geophys. Res., 108, D128527, doi:10.1029/2002JD002596, 2003.

Gerasopoulos, E., Zanis, P., Stohl, A., Zerefos, C. S., Papastefanou, C., Ringer, W., Tobler, L., Huebener, S., Kanter, H. J., Tositti, L., and Sandrini, S.: A climatology of 7Be at four high-altitude stations at the Alps and the Northern Apennines, Atmos. Environ., 35, 6347–6360, 2001.

Gerasopoulos, E., Kouvarakis, G., Vrekoussis, M., Kanakidou, M., and Mihalopoulos, N.: Ozone variability in the marine boundary layer of the Eastern Mediterranean based on 7 year observations, J. Geophys. Res., 110, D15309, doi:10.1029/2005JD005991, 2005.

Gerasopoulos, E., Kouvarakis, G., Vrekoussis, M., Donoussis, C., Mihalopoulos, N., and Kanakidou, M.: Photochemical ozone production in the Eastern Mediterranean. Atmos. Environ., 40, 3057–3069, 2006.

Grell, G. A., Peckham, S. E., Schmitz, R., McKeen, S. A., Frost, G., Skamarock, W. C., and Eder, B.: Fully coupled "online" chemistry within the WRF model, Atmos. Environ., 39, 6957–6975, 2005.

Guenther, A., Karl, T., Harley, P., Wiedinmyer, C., Palmer, P. I., and Geron, C.: Estimates of global terrestrial isoprene emissions using MEGAN (Model of Emissions of Gases and Aerosols from Nature), Atmos. Chem. Phys., 6, 3181–3210, doi:10.5194/acp-6-3181-2006, 2006.

Hijioka, Y., Matsuoka, Y., Nishimoto, H., Matsui, M., and Kanuma, M.: Global GHG emissions scenarios under GHG concentration stabilization targets, Journal of Global Environmental Engineering, 13, 97–108, 2008.

Hjellbrekke, A., Solberg, S., and Fjæraa, A. M.: Ozone measurements 2010 EMEP/CCC-Report 2/2012, available at: http://www.nilu.no/projects/ccc/reports/cccr2-2012.pdf (last access: 13 May 2014), 2012.

Hodnebrog, Ø., Solberg, S., Stordal, F., Svendby, T. M., Simpson, D., Gauss, M., Hilboll, A., Pfister, G. G., Turquety, S., Richter, A., Burrows, J. P., and Denier van der Gon, H. A. C.: Impact of forest fires, biogenic emissions and high temperatures on the elevated Eastern Mediterranean ozone levels during the hot summer of 2007, Atmos. Chem. Phys., 12, 8727–8750, doi:10.5194/acp-12-8727-2012, 2012.

ACPD
14, 12377–12408, 2014

Holton, J. R., Haynes, P. H., McIntyre, E. M., Douglass, A. R., Rood, R. B., and Pfister, L.: Stratosphere–troposphere exchange, Rev. Geophys., 33, 403–439, 1995.
Hurtmans, D., Coheur, P.-F., Wespes, C., Clarisse, L., Scharf, O., Clerbaux, C., Hadji-Lazaro, J., George, M., and Turquety, S.: FORLI radiative transfer and retrieval code for IASI, J. Quant. Spectrosc. Ra., 113, 1391–1408, 2012.
Im, U., Markakis, K., Poupkou, A., Melas, D., Unal, A., Gerasopoulos, E., Daskalakis, N., Kindap, T., and Kanakidou, M.: The impact of temperature changes on summer time ozone and its precursors in the Eastern Mediterranean, Atmos. Chem. Phys., 11, 3847–3864, doi:10.5194/acp-11-3847-2011, 2011.
Kouvarakis, G., Tsigaridis, K., Kanakidou, M., and Mihalopoulos, N.: Temporal variations of surface regional background ozone over Crete Island in the southeast Mediterranean, J. Geophys. Res., 105, 4399–4407, 2000.
Lamarque, J.-F., Hess, P. G., Emmons, L., Buja, L., Washington, W., and Granier, C.: Tropospheric ozone evolution between 1890 and 1990, J. Geophys. Res., 110, D08304, doi:10.1029/2004JD005537, 2005.
Lelieveld, J., Berresheim, H., Borrmann, S., Crutzen, P. J., Dentener, F. J., Fischer, H., Feichter, J., Flatau, P. J., Heland, J., Holzinger, R., Korrmann, R., Lawrence, M. G., Levin, Z., Markowicz, K. M., Mihalopoulos, N., Minikin, A., Ramanathan, V., de Reus, M., Roelofs, G. J., Scheeren, H. A., Sciare, J., Schlager, H., Schultz, M., Siegmund, P., Steil, B., Stephanou, E. G., Stier, P., Traub, M., Warneke, C., Williams, J., and Ziereis, H.: Global air pollution crossroads over the mediterranean, Science, 298, 794–799, doi:10.1126/science.1075457, 2002.
Levy, H. I., Mahlman, J., Moxim, W., and Liu, S.: Tropospheric ozone: the role of transport, J. Geophys. Res., 90, 3753–3772, 1985.
Logan, J. A.: Tropospheric ozone: seasonal behavior, trends, and anthropogenic influence, J. Geophys. Res., 90, 10463–10482, 1985.
Ma, J., Zhou, X., and Hauglustaine, D.: Summertime tropospheric ozone over China simulated with a regional chemical transport model, Part 2. Source contribution and budget, J. Geophys. Res., 107, 4612, doi:10.1029/2001JD001355, 2002.
Pfister, G., Emmons, L. K., Hess, P. G., Honrath, R., Lamarque, J.-F., Val Martin, M., Owen, R. C., Avery, M., Browell, E. V., Holloway, J. S., Nedelec, P., Purvis, R., Rywerson, T. B., Sachse, G. W., and Schlager, H.: Ozone production from the 2004 North American boreal fires, J. Geophys. Res., 111, D24S07, doi:10.1029/2006JD007695, 2006.

ACPD
14, 12377–12408, 2014

Pfister, G. G., Emmons, L. K., Hess, P. G., Lamarque, J.-F., Thompson, A. M., and Yorks, J. E.: Analysis of the summer 2004 ozone budget over the United States using Intercontinental Transport Experiment Ozonesonde Network Study (IONS) observations and Model of Ozone and Related Tracers (MOZART-4) simulations, J. Geophys. Res., 113, D23306, doi:10.1029/2008JD010190, 2008.

Pfister, G. G., Walters, S., Emmons, L. K., Edwards, D. P., and Avise, J.: Quantifying the contribution of inflow on surface ozone over California during summer 2008, J. Geophys. Res.-Atmos., 118, 12282–12299, doi:10.1002/2013JD020336, 2013.

R'Honi, Y., Clarisse, L., Clerbaux, C., Hurtmans, D., Duflot, V., Turquety, S., Ngadi, Y., and Coheur, P.-F.: Exceptional emissions of NH_3 and HCOOH in the 2010 Russian wildfires, Atmos. Chem. Phys., 13, 4171–4181, doi:10.5194/acp-13-4171-2013, 2013.

Richards, N. A. D., Arnold, S. R., Chipperfield, M. P., Miles, G., Rap, A., Siddans, R., Monks, S. A., and Hollaway, M. J.: The Mediterranean summertime ozone maximum: global emission sensitivities and radiative impacts, Atmos. Chem. Phys., 13, 2331–2345, doi:10.5194/acp-13-2331-2013, 2013.

Rodwell, M. J. and Hoskins, B. J.: Monsoons and the dynamics of deserts, Q. J. Roy. Meteor. Soc., 122, 1385–1404, doi:10.1002/qj.49712253408, 1996.

Safieddine, S., Clerbaux, C., George, M., Hadji-Lazaro, J., Hurtmans, D., Coheur, P.-F., Wespes, C., Loyola, D., Valks, P., and Hao, N.: Tropospheric ozone and nitrogen dioxide measurements in urban and rural regions as seen by IASI and GOME-2, J. Geophys. Res.-Atmos., 118, 10555–10566, 2013.

Schubert, S., Wang, H., and Suarez, M.: Warm season sub-seasonal variability and climate extremes in the Northern Hemisphere: the role of stationary Rossby waves, J. Climate, 24, 4773–4792, 2011.

Stohl, A., Spichtinger-Rakowsky, N., Bonasoni, P., Feldmann, H., Memmesheimer, M., Scheel, H. E., Trickl, T., Hubener, S. H., Ringer, W., and Mandl, M.: The influence of stratospheric intrusions on alpine ozone concentrations, Atmos. Environ., 34, 1323–1354, 2000.

Tuccella, P., Curci, G., Visconti, G., Bessagnet, B., Menut, L., and Park, R. J.: Modeling of gas and aerosol with WRF/Chem over Europe: evaluation and sensitivity study, J. Geophys. Res., 117, D03303, doi:10.1029/2011JD016302, 2012.

Turquety, S., Hurtmans, D., Hadji-Lazaro, J., Coheur, P.-F., Clerbaux, C., Josset, D., and Tsamalis, C.: Tracking the emission and transport of pollution from wildfires using the IASI

CO retrievals: analysis of the summer 2007 Greek fires, Atmos. Chem. Phys., 9, 4897–4913, doi:10.5194/acp-9-4897-2009, 2009.

Wespes, C., Emmons, L., Edwards, D. P., Hannigan, J., Hurtmans, D., Saunois, M., Coheur, P.-F., Clerbaux, C., Coffey, M. T., Batchelor, R. L., Lindenmaier, R., Strong, K., Weinheimer, A. J., Nowak, J. B., Ryerson, T. B., Crounse, J. D., and Wennberg, P. O.: Analysis of ozone and nitric acid in spring and summer Arctic pollution using aircraft, ground-based, satellite observations and MOZART-4 model: source attribution and partitioning, Atmos. Chem. Phys., 12, 237–259, doi:10.5194/acp-12-237-2012, 2012.

Wiedinmyer, C., Akagi, S. K., Yokelson, R. J., Emmons, L. K., Al-Saadi, J. A., Orlando, J. J., and Soja, A. J.: The Fire INventory from NCAR (FINN): a high resolution global model to estimate the emissions from open burning, Geosci. Model Dev., 4, 625–641, doi:10.5194/gmd-4-625-2011, 2011.

Zanis, P., Hadjinicolaou, P., Pozzer, A., Tyrlis, E., Dafka, S., Mihalopoulos, N., and Lelieveld, J.: Summertime free-tropospheric ozone pool over the eastern Mediterranean/Middle East, Atmos. Chem. Phys., 14, 115–132, doi:10.5194/acp-14-115-2014, 2014.

Zbinden, R. M., Thouret, V., Ricaud, P., Carminati, F., Cammas, J.-P., and Nédélec, P.: Climatology of pure tropospheric profiles and column contents of ozone and carbon monoxide using MOZAIC in the mid-northern latitudes (24° N to 50° N) from 1994 to 2009, Atmos. Chem. Phys., 13, 12363–12388, doi:10.5194/acp-13-12363-2013, 2013.

ACPD
14, 12377–12408, 2014

Table 1. List of EMEP O_3 monitoring stations used in this study.

Code	Station name	Latitude (° N)	Longitude (° E)	Altitude (m)
CY01	Ayia Marina	35.04	33.06	532
ES06	Mahón	39.87	4.32	78
ES07	Víznar	37.30	−3.53	1265
ES10	Cabo de Creus	42.32	3.32	23
ES12	Zarra	39.08	−1.10	885
ES14	Els Torms	41.39	0.73	470
GR02	Finokalia	35.31	25.66	250
MK07	Lazaropole	41.32	20.42	1332

ACPD
14, 12377–12408, 2014

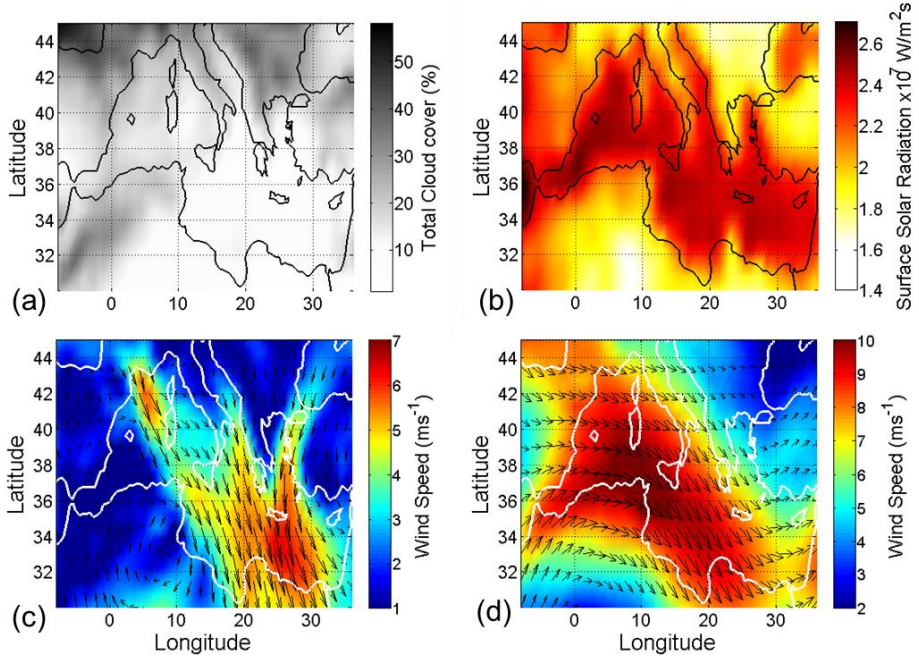

Fig. 1. A representative example of the ECMWF (European Centre for Medium-Range Weather Forecasts) Reanalysis (ERA-Interim) for the period June-July-August (JJA) 2010 for: **(a)** total cloud coverage, **(b)** 12:00 UTC solar radiation reaching the surface and **(c)** wind speed and direction averaged from the surface to 750 hPa and **(d)** wind speed and direction averaged from 750 to 400 hPa.

ACPD
14, 12377–12408, 2014

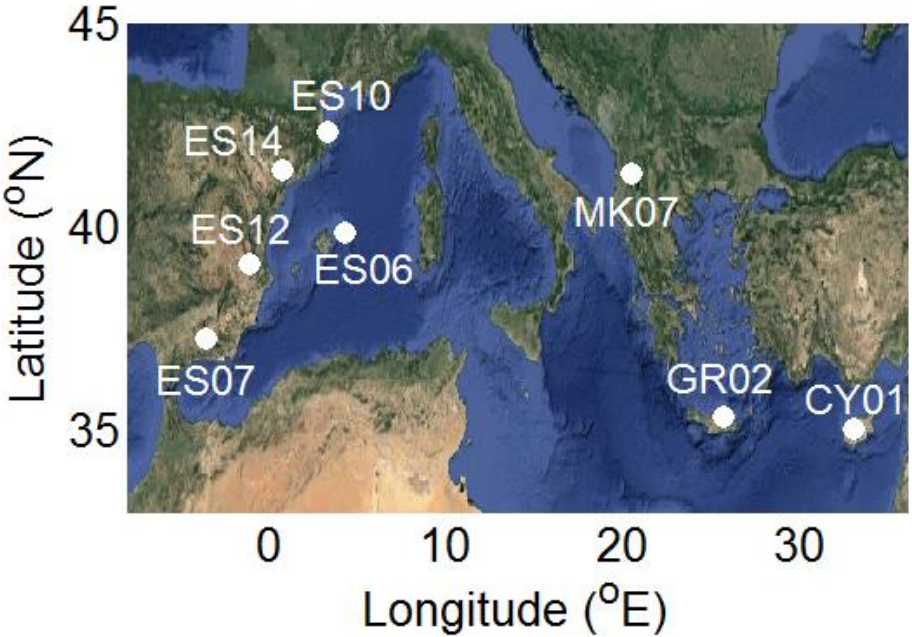

Fig. 2. Location of the EMEP stations used to validate the WRF-Chem model.

ACPD
14, 12377–12408, 2014

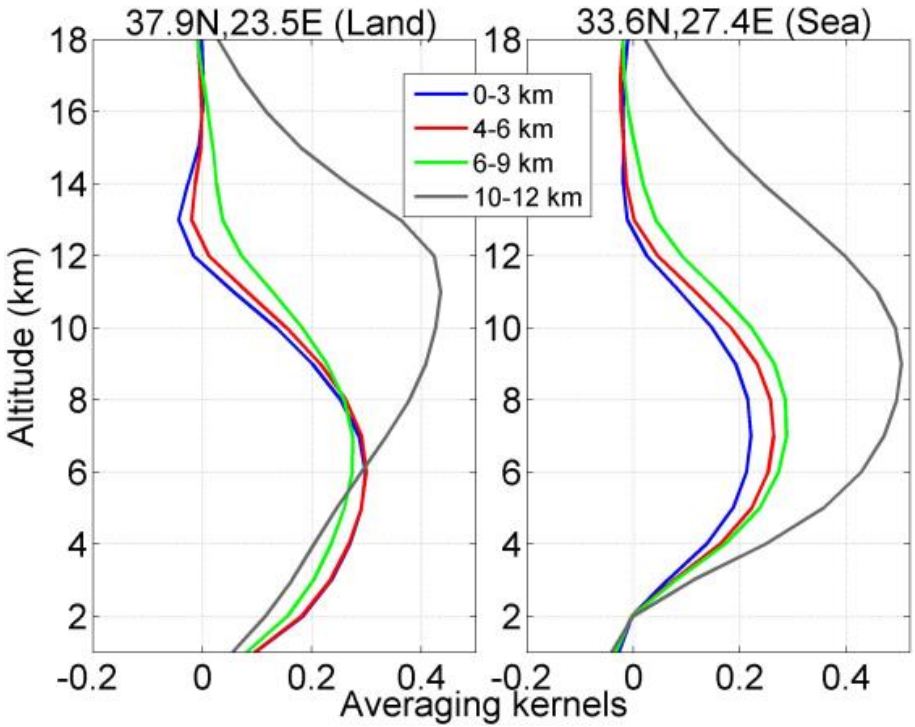

Fig. 3. Typical O_3 averaging kernel over the Mediterranean: the functions are for the [surface-3], [4–6], [6–9], and [10–12] km partial columns characterizing a retrieval for an observation chosen randomly above land (Greece, left panel) and above the sea (right panel) during June 2010.

ACPD
14, 12377–12408, 2014

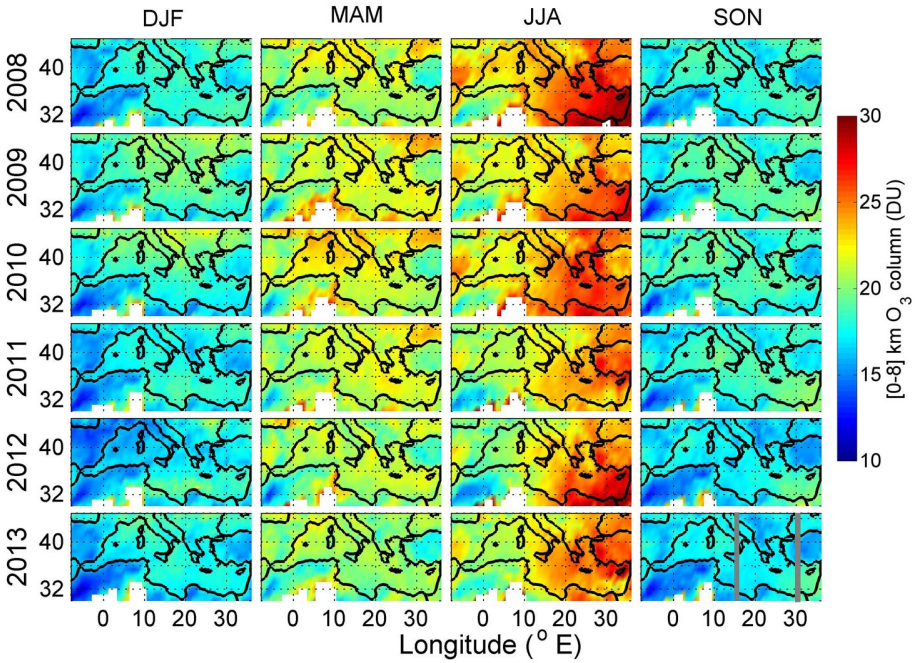

Fig. 4. Six years seasonal variation of [0–8] km integrated IASI O_3 column over the Mediterranean region for winter, spring, summer and autumn. White pixels correspond to a filter applied on poor spectral fits, because of emissivity issues in the FORLI radiative transfer above the Sahara desert. The grey strips in the last panel are the longitude lines used to plot Fig. 5.

ACPD
14, 12377–12408, 2014

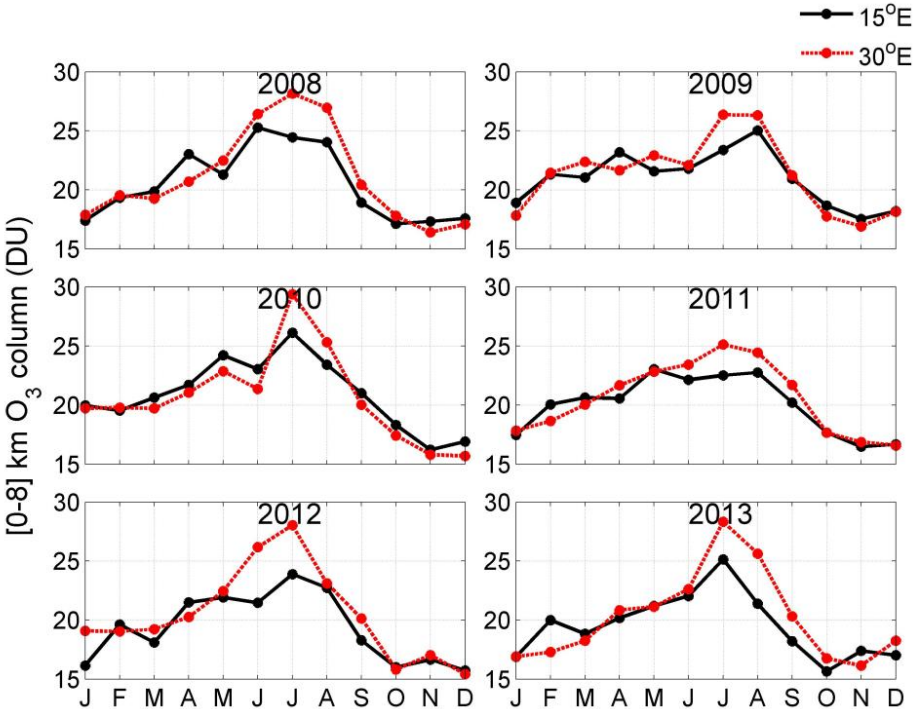

Fig. 5. Six years monthly variation of the integrated [0–8] km IASI O_3 column averaged over [30–45° N] at 15° E (in black) and 30° E (in red). Higher summer values are observed to the east of the basin at 30° E.

ACPD
14, 12377–12408, 2014

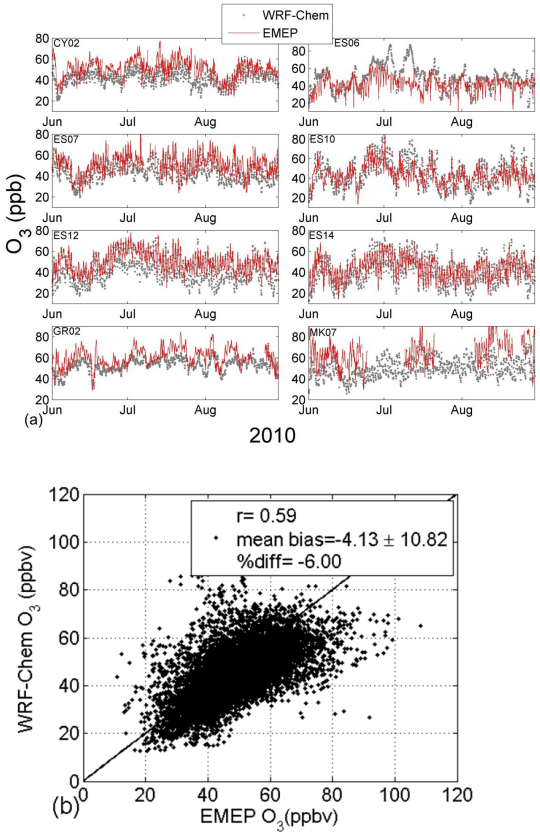

Fig. 6. (a) O_3 time series and **(b)** correlation for EMEP and WRF-Chem data at the surface for the stations localized in Fig. 2, for the period JJA 2010.

ACPD
14, 12377–12408, 2014

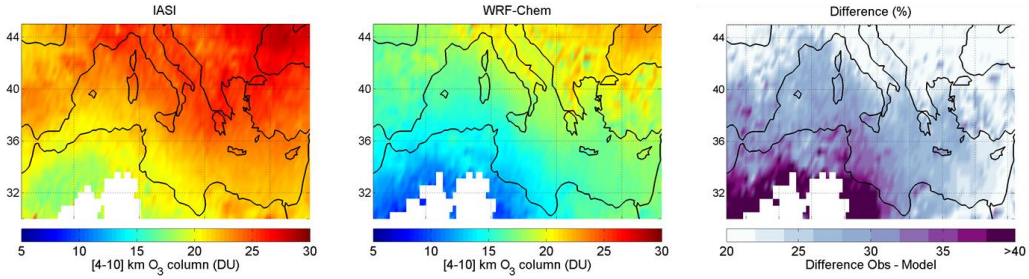

Fig. 7. Average [4–10] km O_3 column for JJA 2010 from IASI and WRF-Chem and their relative difference (%). White pixels correspond to a filter applied to poor spectral fits above the Sahara desert.

ACPD
14, 12377–12408, 2014

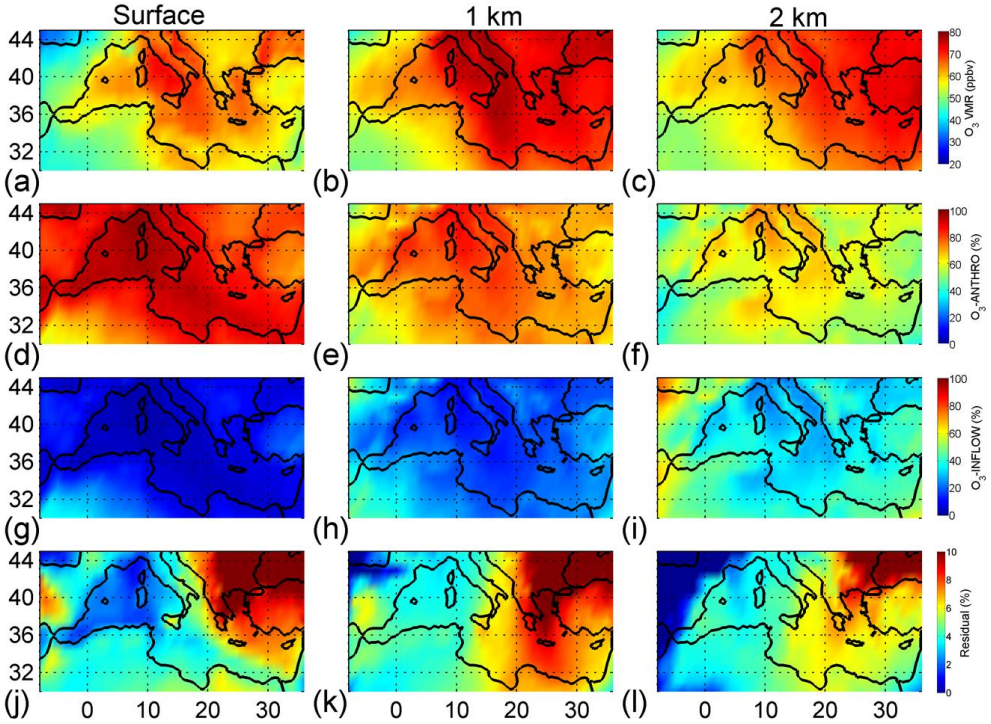

Fig. 8. WRF-Chem spatial distributions of **(a–c)** O_3 mixing ratios (ppbv), **(d–f)** O_3 anthropogenic tracer relative contributions (%), **(g–i)** O_3 inflow tracer relative contribution, and **(j–l)** the residual ($100\,\% - (O_{3_{anthro}}\,\% + O_{3_{inflow}}\,\%)$) averaged over the period JJA 2010 at the surface, 1 km and 2 km.

ACPD
14, 12377–12408, 2014

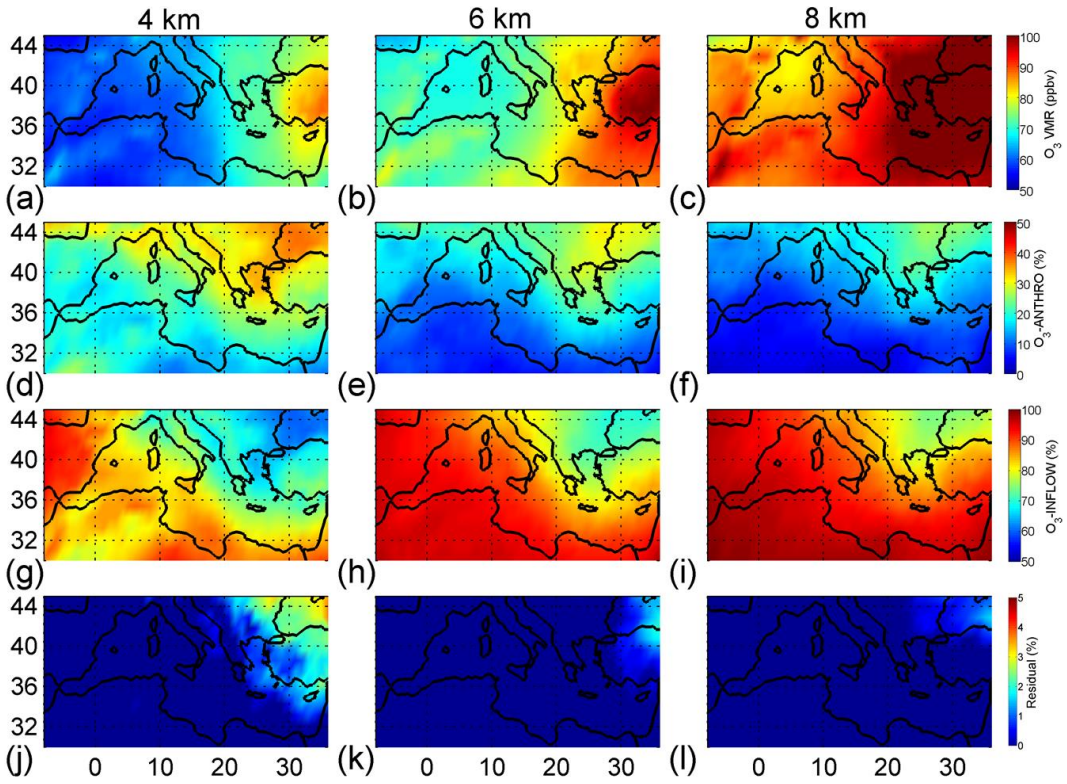

Fig. 9. Same as Fig. 8 but for 4, 6 and 8 km.

ACPD
14, 12377–12408, 2014

Summertime tropospheric ozone assessment over the Mediterranean region

S. Safieddine et al.

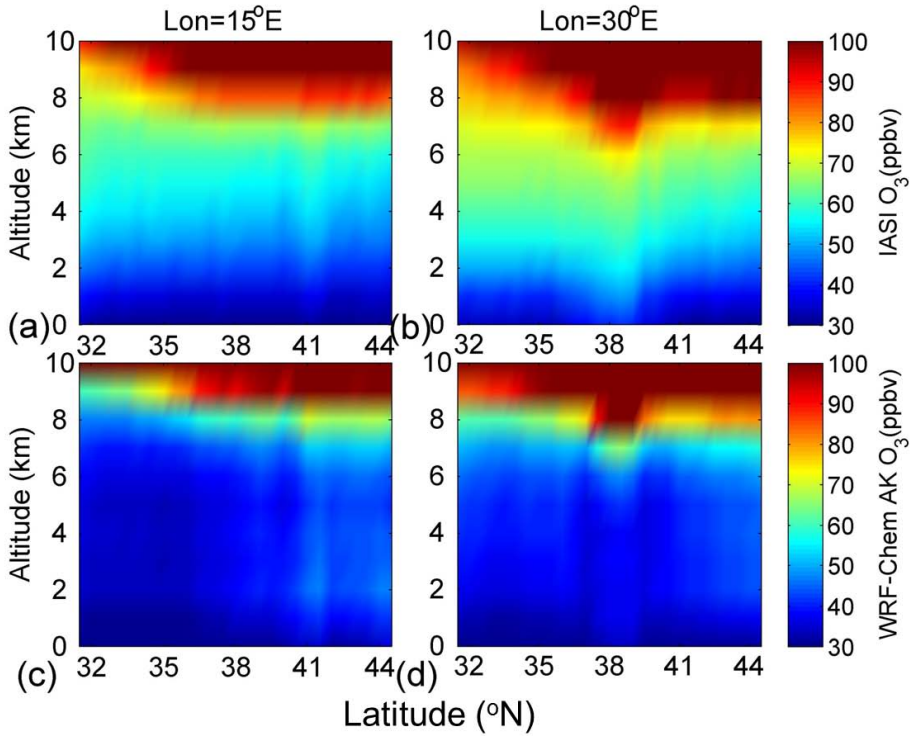

Fig. 10. Mean latitude-altitude cross sections of IASI-O_3 **(a, b)** and modeled-O_3 **(c, d)** averaged over JJA 2010 along 15° E and 30° E. The eastern part of the basin at 30° E is subject to higher STE events.

ACPD
14, 12377–12408, 2014

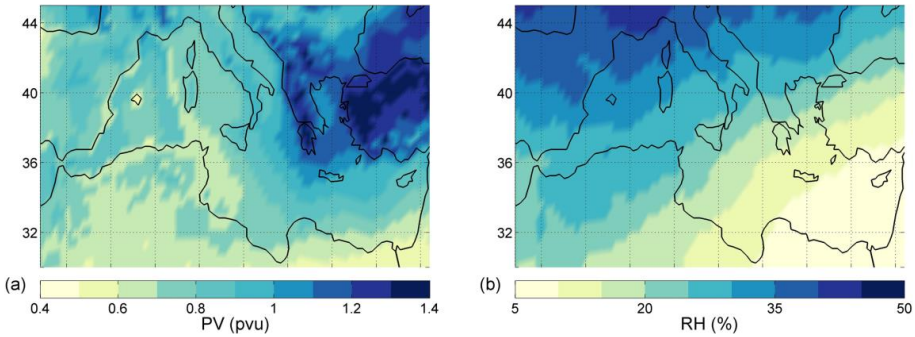

Fig. 11. WRF-Chem **(a)** potential vorticity between 350–250 hPa over the Mediterranean region for JJA 2010 and **(b)** relative humidity for the same vertical levels and time period.

ACPD
14, 12377–12408, 2014